applied sciences

MDPI

Article

Assessing Extreme Drought Events and Their Temporal Impact: Before and after the Operation of a Hydropower Plant

Andrés F. Villalba-Barrios [1], Oscar E. Coronado Hernández [2], Vicente S. Fuertes-Miquel [3,*], Alfonso Arrieta-Pastrana [2] and Helena M. Ramos [4]

[1] Facultad de Ingeniería, Universidad Tecnológica de Bolívar, Cartagena 131001, Colombia; villalbaa@utb.edu.co
[2] Instituto de Hidráulica y Saneamiento Ambiental, Universidad de Cartagena, Cartagena 130001, Colombia
[3] Departamento de Ingeniería Hidráulica y Medio Ambiente, Universitat Politècnica de València, 46022 Valencia, Spain
[4] Department of Civil Engineering, Architecture and Georesources, CERIS, Instituto Superior Técnico, University of Lisbon, 1049-001 Lisbon, Portugal
* Correspondence: vfuertes@upv.es

Abstract: The probabilistic analysis of streamflow and drought event durations plays a crucial role in the efficient and sustainable management of existing water resources in the region. This approach involves the collection of historical hydrological data from river gauging stations, the use of statistical and probabilistic models, and the assessment of hydrological projections at different return periods to provide valuable information for society to understand the potential impacts of extreme events. The analysis is carried out on the Sinú River in Colombia, with consideration given to both the presence and absence of the Hydropower Plant Urrá I. The results reveal that, under natural conditions, a higher number of return periods correspond to less extreme drought flows and longer temporal durations. However, when the hydropower plant is operational, the occurrence and duration of drought are influenced by the regulations implemented during energy generation. The results of this analysis can guide water resource management policies, considering the operation of the hydroelectric plant, thereby enabling decisions that enhance the resilience and sustainability of the river's hydrological conditions and communities that depend on it.

Keywords: low flows; drought hydrograph; statistical analysis; hydropower effect

Citation: Villalba-Barrios, A.F.; Coronado Hernández, O.E.; Fuertes-Miquel, V.S.; Arrieta-Pastrana, A.; Ramos, H.M. Assessing Extreme Drought Events and Their Temporal Impact: Before and after the Operation of a Hydropower Plant. *Appl. Sci.* **2024**, *14*, 1692. https://doi.org/10.3390/app14051692

Academic Editor: Nathan J. Moore

Received: 30 December 2023
Revised: 2 February 2024
Accepted: 18 February 2024
Published: 20 February 2024

1. Introduction

In a glance at continental climate, it is understood that continental climates have different climatic regimes, with occasional transitions between them. These transitions could influence the occurrence of prolonged droughts, along with temporary events of moisture variations in the climate lasting for extended periods [1].

The onset of droughts in large continental regions is primarily related to anomalous features in the planet's atmospheric circulation. Therefore, predictions of drought occurrences have received significant attention, especially concerning the estimation of drought durations [2]. The reasons for drought events are so diverse that simulating the direct evolution of the physical processes leading to them is complex. Jorome Namia describes this by stating that, as is the case with many meteorological and climatological phenomena, there is not a single cause but multiple factors influencing the occurrence of drought [3].

From the above, the analysis of the historical time series of recorded drought data becomes relevant. Through statistical analysis, expected future values of droughts can be provided [2], offering information for decision-making regarding the comprehensive management of water resources in the study area.

In Colombia, due to the atmospheric climate variability, there is significant interannual variability in precipitation, represented by the cycles of La Niña and El Niño. These phe-

nomena have been responsible for extreme rainfall and prolonged droughts, respectively, in the national territory and extending to other continental regions [4].

The definition of drought varies based on specific factors relevant to each location on the planet. However, in general terms, a drought can be described as the insufficient availability of water for anthropic and/or natural activities [5]. According to these anthropic and/or natural requirements, several types of droughts have been identified, each characterized by a significant variation in water demand. These categories include meteorological drought, hydrological drought, agricultural drought, and socio-economic drought [6].

Meteorological drought is defined as a precipitation deficit compared with the water demand of a region [7]. It is typically time-limited, with its duration determining its severity. Agricultural drought refers to the insufficient soil moisture required to support plant life, hindering growth and production. Hydrological drought involves abnormal decreases in minimum river flows, as well as reductions in water volumes stored in lakes and reservoirs, drops in the water table level, and diminished contributions from groundwater [8–10]. Socio-economic drought occurs when water shortage substantially impacts the economic production of communities in the affected territories, thereby affecting their sustainability [6].

Contemporary hydrology requires a comprehensive understanding of all physical processes to facilitate the efficient management of water resources. However, the existing technical conceptualization might not be suitable for assessing various extreme scenarios given that water management has historically prioritized abundance over scarcity or drought [11]. A flood hydrograph is a graphical representation illustrating the river's reaction to rainfall and aquifer contributions [12]. Conversely, a drought hydrograph is a graph that portrays the river's response to the lack of rainfall, depicting minimum flow rates where the only contributors are the aquifer or upstream reservoirs at the measurement point.

Gaining insights into the future hydrological dynamics of rivers and bodies of water has long been a goal of humanity. Consequently, understanding the patterns of the dry season in the Sinú River holds significance. This research study seeks to estimate extreme dry events for varying return periods, furnishing robust information to support comprehensive water management that addresses abundance (floods) and scarcity (droughts). This study provides estimations of minimum flow rates and durations of droughts across different return periods, unveiling the probable magnitude of extreme dry events. All these considerations involve constructing drought hydrographs that depict this physical phenomenon in the Sinú River, specifically at the Montería Automatic limnigraphic station. This research holds significant importance for water resources management in Colombia, particularly due to the scarcity of gauging stations. Consequently, the operation of the Urrá I Hydropower Plant can change extreme droughts in the Sinú River.

2. Case Study

This study focuses on the Sinú River basin, encompassing a drainage area of 13,952 km^2 and a length of 437.97 km (see Figure 1). The basin covers territories in three Colombian departments—Antioquia, Sucre, and Córdoba—ultimately discharging into the Caribbean Sea waters in the municipality of San Bernardo del Viento. The datasets used in this research were sourced from the limnigraphic station on the Sinú River known as the "Montería Automatic" station. This station is located at latitude 8.751611111 and longitude −75.8924166, with the station code 13067020. It is operated by the Colombian Institute of Hydrology, Meteorology, and Environmental Studies (IDEAM) [13]. The limnigraphic station includes the hydrological effects caused by the Urrá I Hydropower Plant, which is situated in the northwestern region of Colombia, approximately 30 km south of the municipality of Tierralta in the department of Córdoba. The dam consists of a central core of clayey gravel, standing at a height of 73 m. Its spillway, constructed of concrete, has a maximum discharge capacity of around 9000 m^3/s.

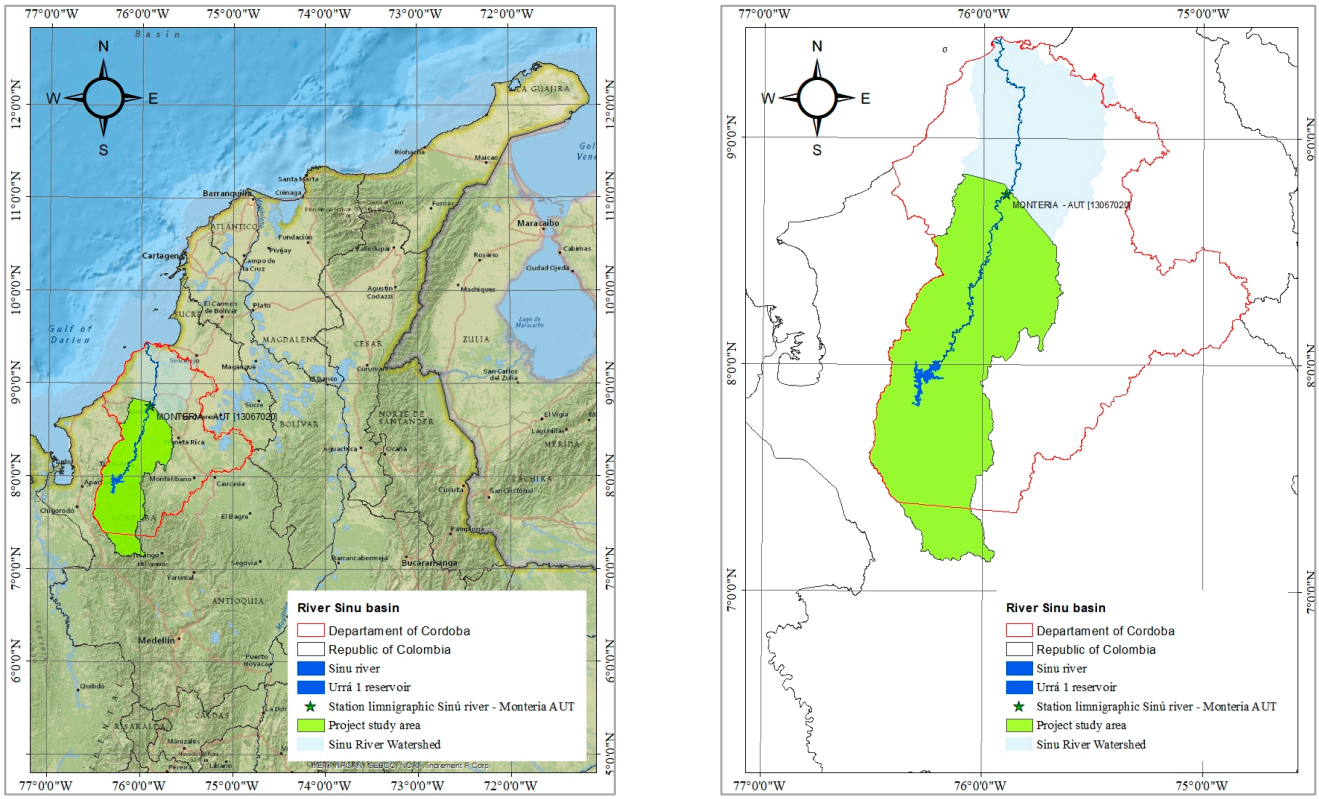

(**a**) (**b**)

Figure 1. Location of the Montería Automatic limnigraphic station: (**a**) geographic location of the study area; and (**b**) hydrographic basin of the Sinú River up to the station.

3. Materials and Methods

3.1. Available Information

The collected data comprise daily gauged streamflow data from the Montería Automatic limnigraphic station on the Sinú River. From these values, the minimum for each year in the measured series is determined. The datasets from 1970 and 1971 were excluded due to limited recorded information in those years (see Table 1), which does not accurately depict the hydrological reality of the river. Q_V represents the minimum streamflow rates.

The multiannual minimum flows exhibit values ranging from 37.50 to 160.00 m^3/s in 1988 and 1985, respectively. The minimum values for 1970 and 1971 were excluded due to a substantial deviation compared with the rest of the dataset. This is attributed to the absence of consistent records over several days in those years.

The sample mean, or sample average, is a value computed from a data sample, considering the data and sample size [14], which is a widely used statistical measure used to determine the midpoint value of the corresponding dataset [15]. The standard deviation was used to identify how far individual values are from the sample mean [15]. The mode was another statistical measure, which refers to the data point that exhibits the highest frequency within the series. Essentially, it is the value that occurs most frequently in the dataset [15]. In summary, the fundamental statistical behavior reveals that the mode of the observed series of multiannual minimum streamflows is 55.60 m^3/s, appearing twice. The sample mean for the minimum streamflow is around 94.65 m^3/s, and the closest observed value to the mean is 93.70 m^3/s in 1974, with a difference of 0.95 (Figure 2). The standard deviation of the dataset is 35.35 m^3/s, and the year closest to the standard deviation is 1983 with a difference of 0.13 (Figure 3). As observed in Figures 2 and 3, the streamflow denoted in Figure 3 exceeds the standard deviation. However, in Figure 2, the streamflow is predominantly below the sample mean.

Table 1. Minimum flows observed during 1972–1999 and 2000–2021.

1972–1999		2000–2021	
Year	**Q_V (m^3/s)**	**Year**	**Q_V (m^3/s)**
1972	75.88	2000	72.40
1973	55.20	2001	118.40
1974	93.74	2002	69.60
1975	54.60	2003	45.00
1976		2004	55.60
1977	44.60	2005	71.00
1978	71.50	2006	75.20
1979	56.20	2007	55.60
1980	46.50	2008	54.20
1981	115.80	2009	62.60
1982	68.00	2010	82.35
1983	58.60	2011	144.35
1984	76.36	2012	137.00
1985	60.00	2013	133.50
1986	70.50	2014	137.00
1987	58.20	2015	133.50
1988	37.50	2016	137.00
1989	67.56	2017	129.25
1990	76.68	2018	130.70
1991	80.00	2019	125.50
1992	44.17	2020	129.50
1993	89.80	2021	130.30
1994	62.25		
1995	102.40		
1996	145.60		
1997	59.00		
1998	51.00		
1999	160.00		

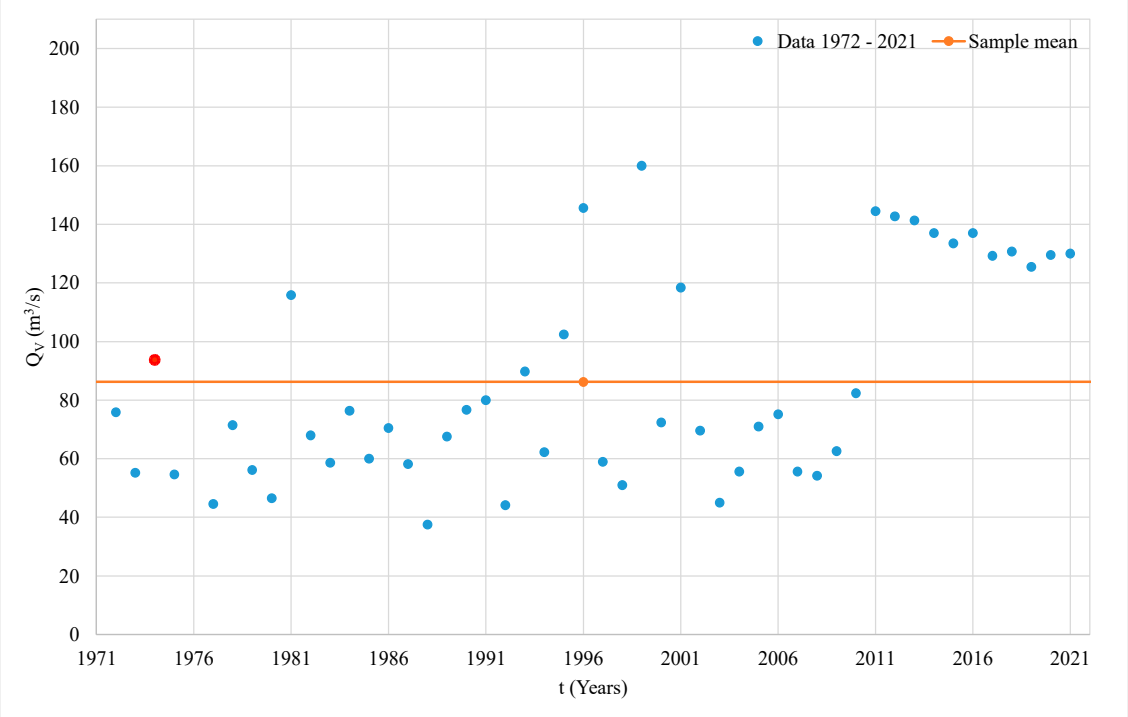

Figure 2. Observed dataset dispersion regarding the sample mean.

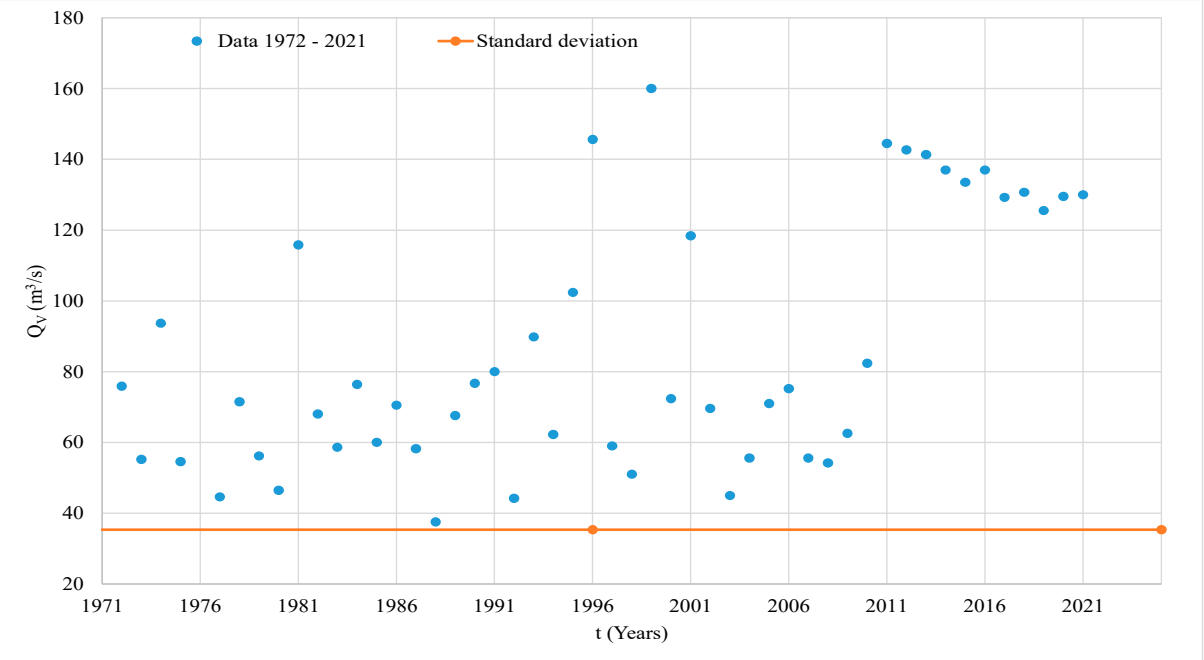

Figure 3. Observed dataset dispersion regarding the standard deviation.

3.2. Drought Hydrographs

Drought hydrographs visually denote streamflow declines, thereby indicating the minimum streamflow values recorded for the corresponding river. These graphs are constructed using datasets collected at specific measurement points, e.g., a limnigraphic station, and are plotted on a chart where the vertical axis represents streamflow and the horizontal axis represents time. These graphical representations facilitate the identification of hydrological drought duration.

In the construction of drought hydrographs based on streamflow data in rivers, the methodological guidelines applied in flood hydrograph generation are used. This involves graphically and numerically determining the duration of the flood and its peak flow, which represents the maximum flow of the flood. From this and with methodological adjustments, annual values of minimum flows (Q_V) in m^3/s and drought durations in days are established. With these identified data, statistical probability distribution methods are then applied for estimation [16].

Comprehending drought hydrographs is essential for efficiently managing available water resources during different seasons. This understanding aids in anticipating water scarcity and implementing mitigation measures to meet human needs in the anticipated extreme event. Figure 4 presents the components to describe a drought hydrograph, where Q_V is the valley streamflow (the minimum value recorded in the dataset for the year under study); V_S represents a volume under the $q_v(t)$ curve; $q_V(t)$ is the curve function described by the drought hydrograph; and $Q_{Reference}$ corresponds to the maximum value streamflow rate of the drought hydrograph.

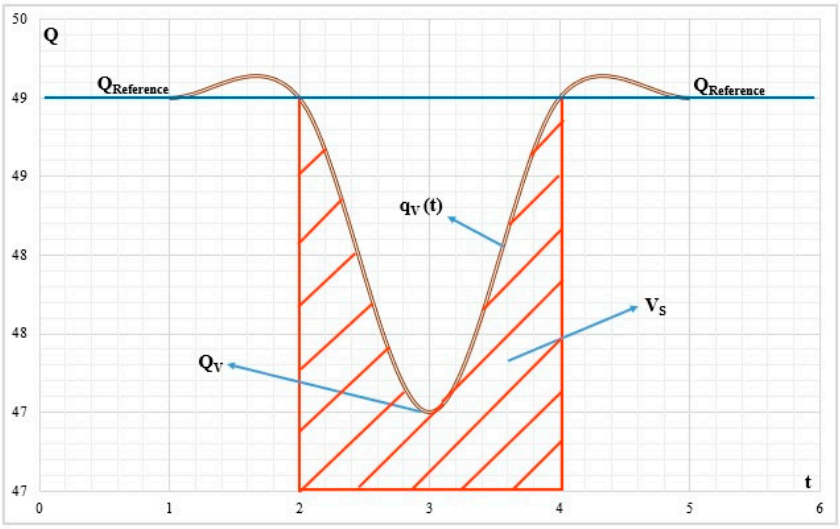

Figure 4. Standard drought hydrograph.

When elaborating the drought hydrographs from Figure 5, the authors considered the datasets from 1972 to 2021 provided by the Montería Automatic station. This involved numerically identifying minimum streamflow values, Q_V, and delimiting the extremes of the hydrograph, including the onset of the descent, the minimum zone, and the rise of the observed streamflows in the river. The hydrometric information available at the Montería Automatic station enables the creation of the graphs shown in Figure 5, highlighting depressions in the river's instantaneous streamflows. Figure A1 presents the total annual drought hydrographs recorded at the Montería Automatic station.

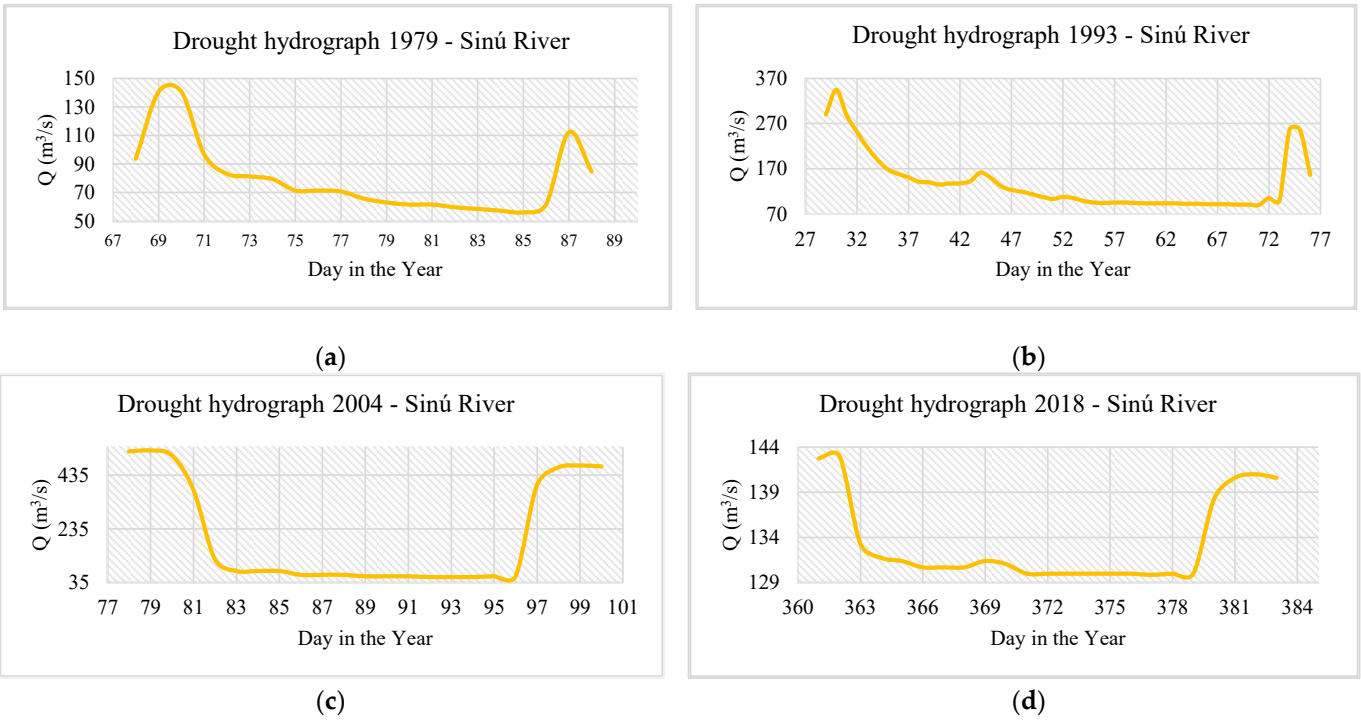

Figure 5. Annual drought hydrograph recorded at the Montería Automatic station from 1972 to 2021. (**a**,**b**) Before the hydroelectric power plant enters operation. (**c**,**d**) After the hydroelectric power plant enters operation.

Each hydrograph represents the maximum drought experienced in the study year, providing insight into the multiannual minimum streamflow or valley streamflow, Q_V (m^3/s), as well as the duration of each dry event in the Sinú River basin.

The minimum streamflow for the entire dataset occurred in 1988 with a streamflow of 37.50 m^3/s, and the maximum minimum streamflow was 160.00 m^3/s, with an average minimum streamflow of 86.22 m^3/s. Concerning durations, there is a minimum drought duration of 6 days in 2010 and a maximum drought duration of 95 days in 1983.

Overall, maximum droughts occurred during the period when the hydroelectric plant was not in operation, while the minimum duration of drought occurred when it was operational.

Time durations were computed considering the drought hydrographs, as shown in Table 2. The periods of 1970–1999 and 2020–2021 were identified in order to neglect and consider the effects produced by the Hydropower Plant Urrá I, respectively.

Table 2. Duration of observed droughts in 1972–1999 and 2000–2021.

1970–1999		2000–2021	
Year	**Duration (Days)**	**Year**	**Duration (Days)**
1972	42	2000	40
1973	40	2001	23
1974	40	2002	47
1975	26	2003	22
1976	Not available	2004	21
1977	88	2005	17
1978	29	2006	11
1979	19	2007	10
1980	80	2008	24
1981	18	2009	13
1982	35	2010	8
1983	97	2011	34
1984	67	2012	22
1985	44	2013	17
1986	50	2014	8
1987	49	2015	15
1988	94	2016	15
1989	26	2017	14
1990	10	2018	21
1991	31	2019	40
1992	55	2020	48
1993	46	2021	54
1994	20		
1995	26		
1996	22		
1997	51		
1998	68		
1999	17		

3.3. Probability Distributions, Fit Methods, and Inferential Statistics

To estimate valley streamflows and drought durations for different return periods, the authors used the probability distributions below in Table 3. These distributions include Weibull [17], Generalized Extreme Value (GEV) [18], Gumbel [19], normal [12], log-normal [20], three-parameter log-normal, gamma, generalized gamma, inverse gamma, Pearson type III [21], and log Pearson type III [20,22].

Table 3. Probability distributions.

Probability Distribution	Formulation	Equation Number
Weibull	$f(x) = \frac{c}{\alpha}\left(\frac{x}{\alpha}\right)^{c-1} exp\left[-\left(\frac{x}{\alpha}\right)^{c}\right]$ $f(x)$: Probability density function, x: Randon variable, α: scale parameter, c: parameter of the distribution.	(1)
GEV	$f(x) = \frac{1}{\alpha}\left[1 - \frac{k}{\alpha}(x-u)\right]^{\frac{1}{k}-1} exp\left\{-\left[1 - \frac{k}{\alpha}(x-u)\right]^{\frac{1}{k}}\right\}$ $f(x)$: Probability density function, x: Randon variable, u: mean of the data, α: scale parameter, k: shape parameter.	(2)
Gumbel	$f(x) = \frac{1}{\alpha} exp\left[-\frac{x-u}{\alpha} - exp\left(-\frac{x-u}{\alpha}\right)\right]$ $f(x)$: Probability, x: Randon variable, u: mean of the data, α: scale parameter	(3)
Normal	$f(x) = \frac{1}{\sigma\sqrt{2\pi}} exp\left\{-\frac{(x-u)^2}{2\sigma^2}\right\}$ $f(x)$: Probability density function, x: Randon variable, u: parameter of the distribution, σ: standard deviation.	(4)
Log-normal	$f(x) = \frac{1}{x\sigma\sqrt{2\pi}} exp\left\{-\frac{(Ln\ x-u)^2}{2\sigma^2}\right\}$ $f(x)$: Probability density function, x: Randon variable, u: parameter of the distribution, σ: standard deviation.	(5)
Three-parameter log-normal	$f(x) = \frac{1}{(x-m)\sigma\sqrt{2\pi}} exp\left\{-\frac{[Ln\ (x-m)-u]^2}{2\sigma^2}\right\}$ $f(x)$: Probability density function, x: Randon variable, m: arithmetic average, u: parameter of the distribution, σ: standard deviation.	(6)
Gamma	$f(x) = \frac{\alpha^{\lambda}}{\Gamma(\lambda)} x^{\lambda-1} e^{-\alpha x}$ $f(x)$: Probability density function, x: Randon variable, Γ: gamma function, α: shape parameter, λ: scale parameter.	(7)
Generalized gamma	$f(x) = \frac{\lvert S\rvert\alpha^{S\lambda}}{\Gamma(\lambda)} x^{S\lambda-1} e^{-(\alpha x)^{S}}$ $f(x)$: Probability density function, x: Randon variable, Γ: gamma function, α: shape parameter, λ: scale parameter, S: standard deviation.	(8)
Inverse gamma	$f(x) = \frac{\alpha^{\lambda}}{\Gamma(\lambda)}\left(\frac{1}{x}\right)^{\lambda+1} e^{-\alpha/x}$ $f(x)$: Probability density function, x: Randon variable, Γ: gamma function, α: shape parameter, λ: scale parameter.	(9)
Pearson type III	$f(x) = \frac{1}{\lvert\alpha\rvert\lambda(k)}(x-\beta)^{k-1} e^{\left[-\frac{(x-\beta)}{\alpha}\right]}$ $f(x)$: Probability density function, x: Randon variable, u: mean of the data, α: scale parameter, k: shape parameter, λ: gamma function, β: location parameter.	(10)
Log Pearson type III	$f(x) = \frac{1}{\lvert\alpha\rvert x\lambda(k)}\left(\frac{Ln\ x-\beta}{\alpha}\right)^{k-1} e^{\left[-\left(\frac{Ln\ x-\beta}{\alpha}\right)\right]}$ $f(x)$: Probability density function, x: Randon variable, u: mean of the data, α: scale parameter, k: shape parameter, λ: gamma function, β: location parameter.	(11)

For the fitting methods, maximum likelihood [23,24], method of moments [12], and weighted method of moments [23] were used. Furthermore, the weighted method of moments and WRC (Water Resources Commission) [25] for the log Pearson type III probability distribution are presented in Table 4.

Table 4. Fitting methods.

Fitting Method	Formulation	Equation Number
Maximum likelihood	$LF = \prod_{i=1}^{n} f(Qv, Tr)$ LF: likelihood function, f: derivative of the logarithm of the function	(12)
Moments	$M_1 = \frac{1}{n}\left(\sum_{i=1}^{n} x_i\right)$ $M_2 = E\left[(x-\mu)^2\right]$ $M_3 = \frac{E\left[(x-\mu)^3\right]}{\sigma^3}$ M_i: Moments, n: data number, x_i: ith data observed, x: data observed, μ: mean, σ: standard deviation, E: expected value operator.	(13)
Weighted moments	$M_0 = \frac{(\sum_{i=1}^{n} x_i)}{n}$ $M_1 = \frac{[\sum_{i=1}^{n} x_i(F1)]}{n}$ $M_2 = \frac{\left[\sum_{i=1}^{n} x_i(F1)^2\right]}{n}$	(14)
Method of moments (BOB)	$M_0 = \frac{(\sum_{i=1}^{n} x_i)}{n}$ M_i: Moments, n: data number, x_i: ith data observed, F_i: is its non-exceedance probability estimated. $M_1 = \frac{[\sum_{i=1}^{n} x_i(F1)]}{n}$ $M_2 = \frac{\left[\sum_{i=1}^{n} x_i(F1)^2\right]}{n}$ M_i: Moments, n: data number, x_i: ith data observed, F_i: is its non-exceedance probability estimated.	(15)
WRC	$W = \frac{V_m}{V_s+V_m}$ W: weighting coefficient, V_s: true variance, V_m: minimum variance.	(16)

Inferential statistics serve as criteria for selecting the best-fitting probability distribution for the data under study. In this research, the authors considered the Chi-square statistic, the coefficient of variation, the kurtosis coefficient, the skewness coefficient, as well as the AIC.

The Chi-square statistic is widely used to assess the existence of a relationship or discrepancy between observed and expected data in a dataset, where the recorded frequency is compared with its expected projection.

In hypothesis testing, the Chi-square is calculated by comparing the observed frequencies in a dataset with the frequencies that would be expected if there were no significant associations between the variables.

If the discrepancy between the observed and expected frequencies is substantial, it can be concluded that there is a significant association between the variables, thus leading to the rejection of the null hypothesis (H_0).

In this case, we could propose two hypotheses. The null hypothesis, H_0, suggests no statistical association between the observed valley streamflows, Q_V, and valley streamflows for different return periods, $Q_{V,Tr}$. Alternatively, H_1 establishes a statistical association between Q_V and Q_{VTr} [23,26]. The coefficient of variation, C_V [12], measures the variability in a data sample in relation to its mean value. The skewness coefficient, C_S [12], assesses the symmetry of the data, measuring the third moment around the mean, indicating the direction and magnitude in which the tail of the distribution extends to the right or left relative to its mean value. If the tail is to the left, it is called negative skewness, and if it is to the right, it is called positive skewness. The kurtosis coefficient, C_K [27], is a statistical measure used to describe the shape of the probability distribution of a dataset. It indicates the data distribution around the mean and the comparison between the tails of the distribution and the shape of the normal distribution. A positive kurtosis coefficient, C_K, is

known as leptokurtic, zero kurtosis is called mesokurtic, and a negative kurtosis is referred to as platykurtic.

The Akaike Information Criterion (AIC) [28,29] is primarily used to compare several models and select the one with the lowest value. A lower AIC value indicates a better balance between model fit and complexity. However, the AIC does not provide an absolute measure of how well a model fits the data; it is used in comparison with other alternative models. Therefore, the AIC serves as a tool for choosing statistical models based on the goodness of fit and complexity (see Table 5).

Table 5. Statistics.

Statistics	Formulation	Equation Number
X^2: Chi-squared	$X^2 = \sum_{i=1}^{K} \left[\frac{(O_i - E_i)^2}{E_i} \right]$ X^2: Chi-square statistic, O_i: is the observed number of events in the ith sub-interval, E_i: is the number of events, k: is an integer number for sub-intervals.	(17)
C_V: Coefficient of variation	$C_V = \frac{\left[\frac{1}{n-1}\sum_{i=1}^{n}(x_i - \overline{x})^2\right]^{1/2}}{\frac{1}{n}\sum_{i=1}^{n} x_i}$ C_v: coefficient of variation, x_i: observed variable, $\overline{x}$: arithmetic average, n: data number.	(18)
C_s: Skewness coefficient	$C_s = \frac{n\sum_{i=1}^{K}(x_1 - \overline{x})^3}{(n-1)(m-2)s^3}$ C_v: skewness coefficient, x_i: observed variable, $\overline{x}$: arithmetic average, n: data number, k: number of classes, m: mode.	(19)
C_K: Kurtosis coefficient	$C_K = \frac{\sum(x_i - \overline{x})^4 / n}{S^4}$ C_k: kurtosis coefficient, x_i: observed variable, $\overline{x}$: arithmetic average, n: data number, S: standard deviation.	(20)
Akaike Information Criterion (AIC)	$AIC_i = -2LogL_i + 2V$ L_i: the maximized value of the likelihood function for the model, V_i: number of parameters	(21)

3.4. Methodological Flow Chart

Figure 6 illustrates the flowchart used in this study, outlining each step of the adopted methodology. The process involves collecting information for analysis based on minimum streamflows, followed by trend analysis, and fitting for different return periods.

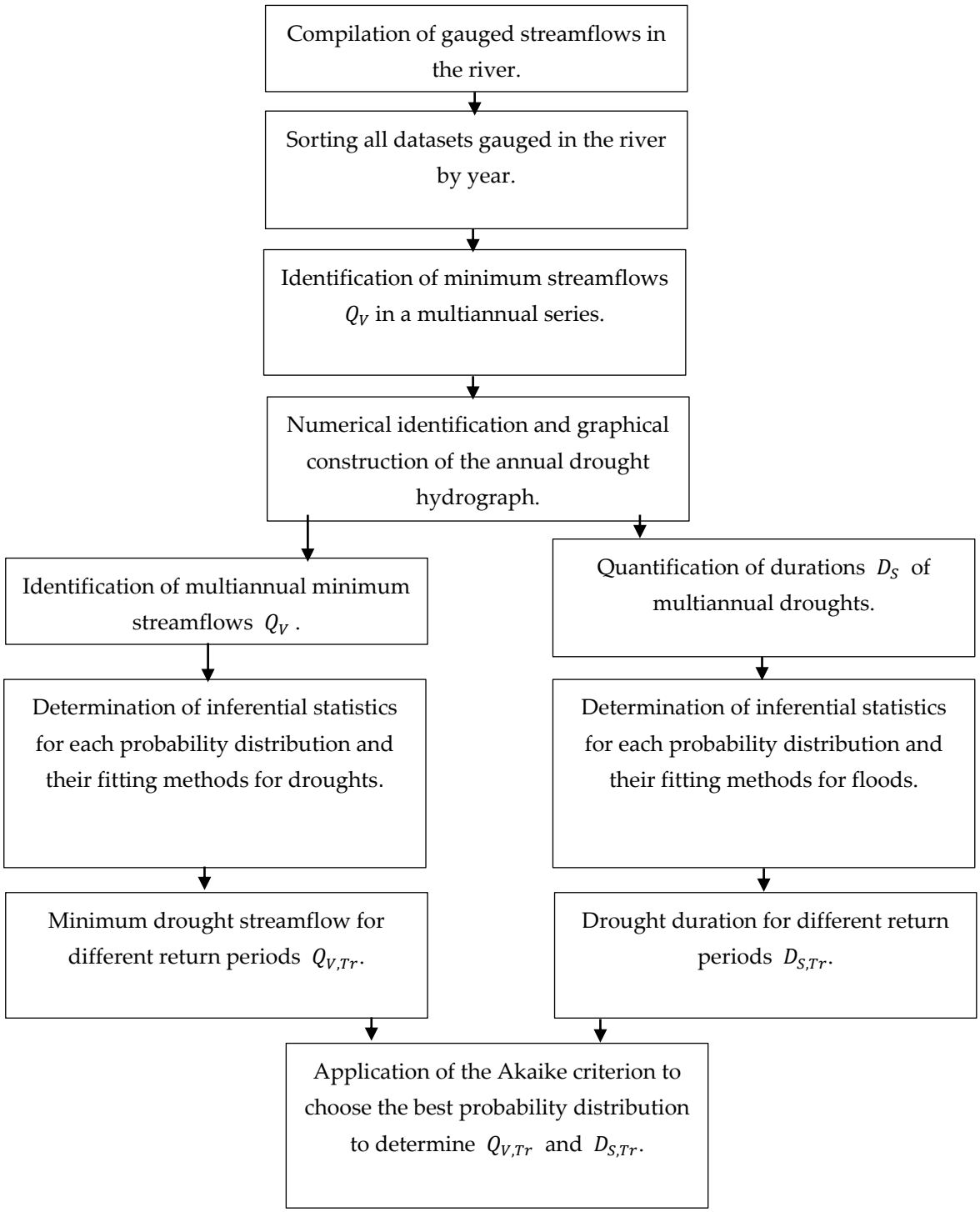

Figure 6. Methodological flowchart.

4. Results

4.1. Minimum Streamflows Q_V and Drought Durations

From all the daily gauged records, the minimum value for each year was determined. It is important to note that the minimum streamflows, Q_V, during 1972–1999 represent a time frame illustrating the hydrological behavior of the Sinú River before the operation of the Urrá 1 hydroelectric plant. The gauged values range from 160 m^3/s in 1985 for the maximum base flow to 37.50 m^3/s in 1988 for the minimum streamflow, Q_V, within the period.

The red line represents a linear trendline of the data, revealing that multiannual minimum streamflows, Q_V, exhibit a gentle upward trend over the recorded years.

In the 2000 to 2021 period, during which the Urrá 1 hydroelectric plant was in operation, the data show an upward trend line over the years. The maximum minimum value is shown in the year 2011, reaching 144 m^3/s, while the minimum value reported is 45 m^3/s in 2003. This increasing trend is attributed to the rise in minimum river streamflows, Q_V, sustained by the operation of the hydroelectric plant. During dry periods, in addition to groundwater contributions, the plant provides a significant additional flow, especially from 2011 until the end of the series in 2021.

Figure 7 presents the trend where the hydroelectric power plant was not yet in operation (period from 1972 to 1999), in contrast to Figure 8, it is evident that the minimum streamflows of the river, Q_V, denote a significant increase, especially from 2011, where all flows above 100 m^3/s are observed.

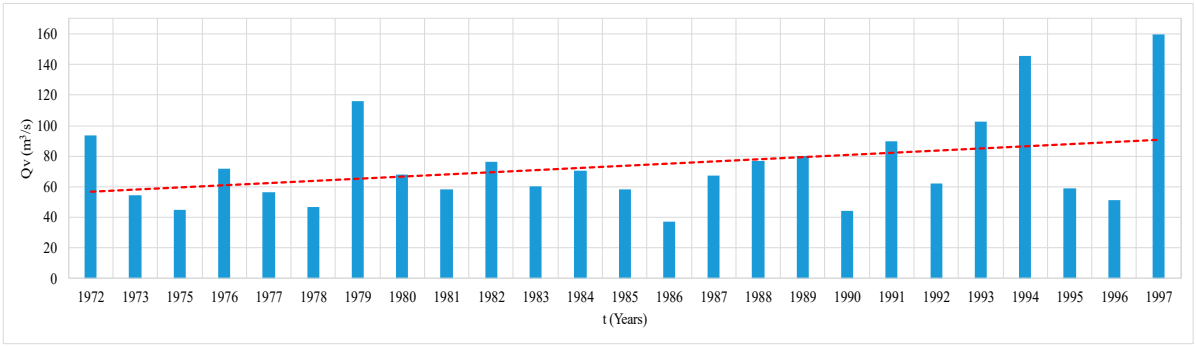

(**a**)

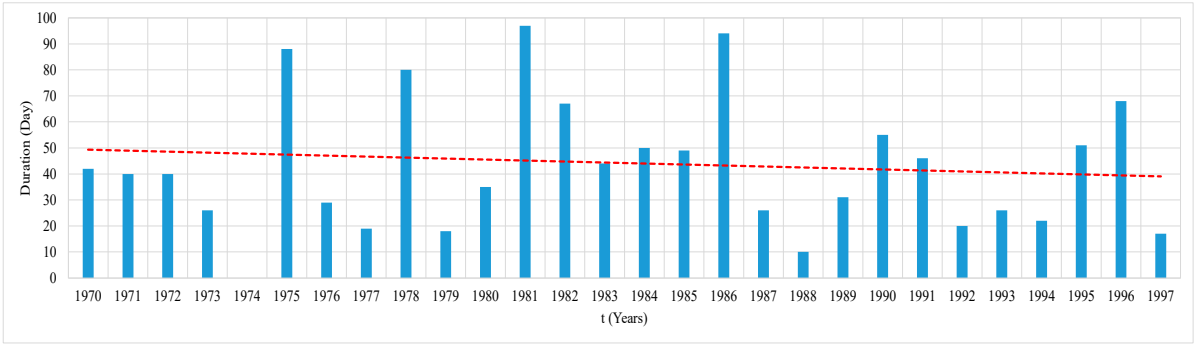

(**b**)

Figure 7. Trends of analyzed variables during 1972–1999: (**a**) multiannual minimum streamflow, Q_V; and (**b**) multiannual drought duration, D_S, record.

Figure 9 depicts the natural hydrological behavior without the operation of the hydroelectric plant, illustrating the relationship between the base flows, Q_V, of the river and its contributing aquifers. The larger the drought duration, the lower the streamflow, Q_V, is reached by the Sinú River.

In the period between 2000 and 2021, during the operation of the Urrá 1 hydroelectric plant, two groups of data are clearly observed. One group, shown in orange, is predominantly located in the lower part of Figure 10, while the other group, illustrated in blue, is entirely situated in the upper part of Figure 10. This indicates two operating policies of the hydroelectric plant: one represented by the orange data from 2000 to 2010 and another represented by the blue data from 2011 to 2021. The latter period denoted higher minimum streamflows, Q_V, in the Sinú River.

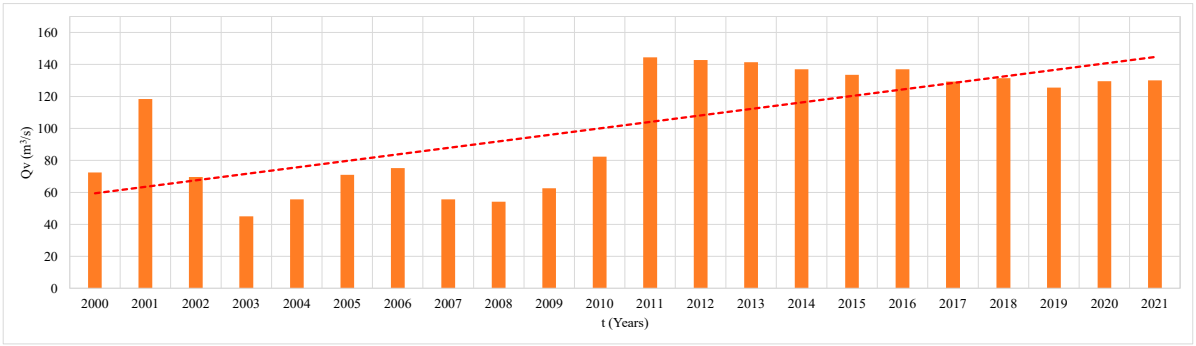

(**a**)

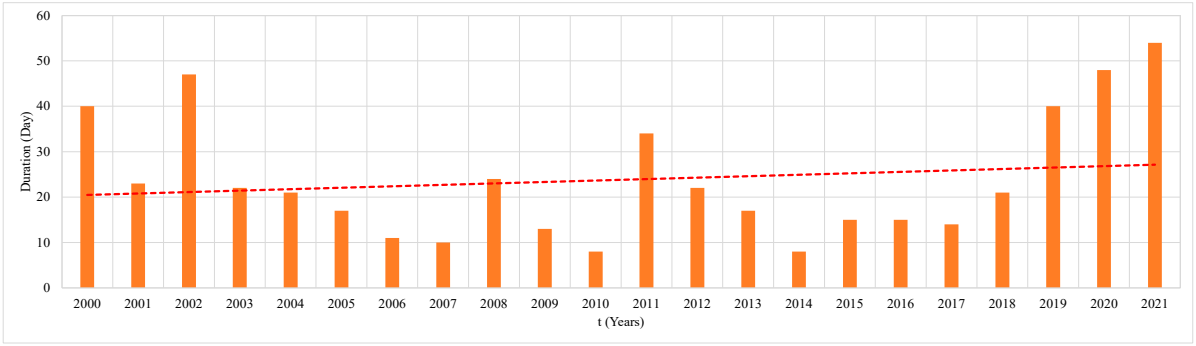

(**b**)

Figure 8. Trends of analyzed variables during 2020–2021: (**a**) Multiannual monthly minimum streamflow, Q_V; and (**b**) drought duration record.

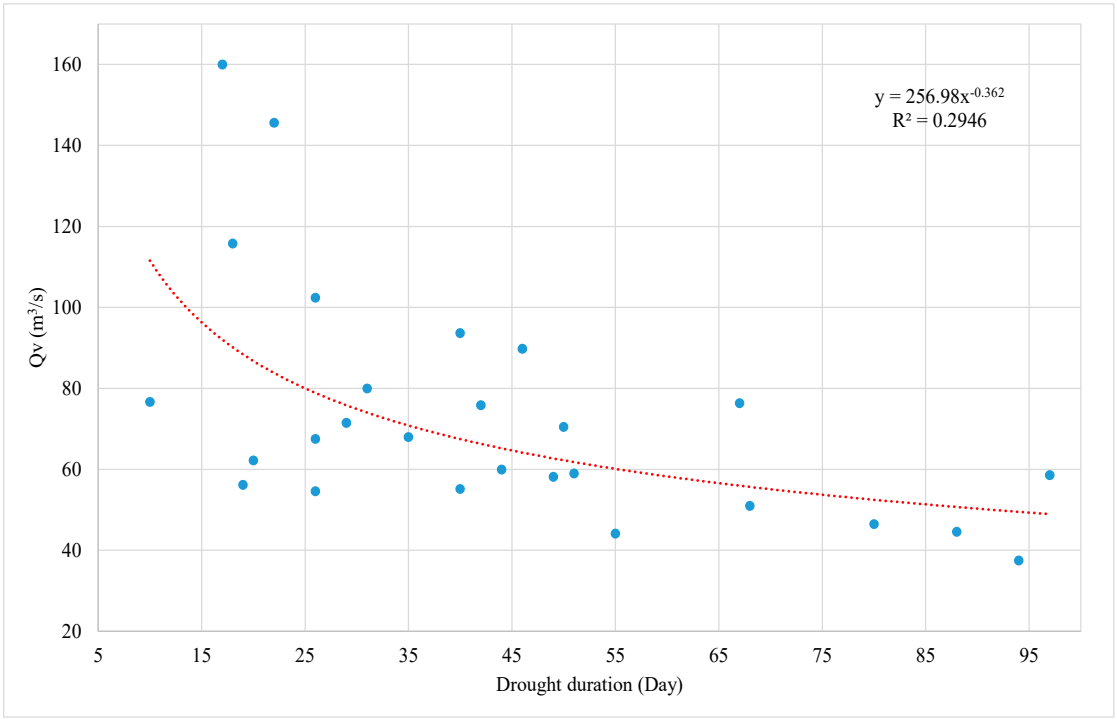

Figure 9. Multiannual monthly minimum streamflow, Q_V, versus drought duration, D_S, record during 1970–1999.

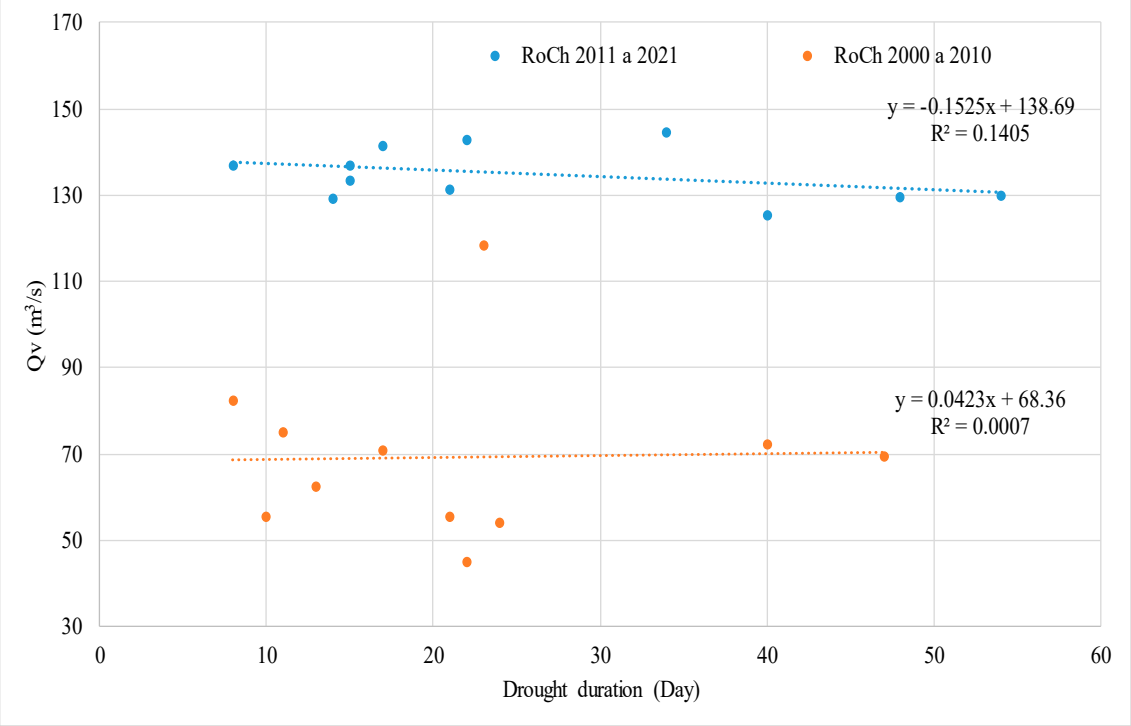

Figure 10. Multiannual monthly valley streamflow versus drought duration, D_S, record during 2000–2021.

4.2. Extreme Values for Different Return Periods

4.2.1. Minimum Streamflows Q_V

For the period 1972–1999, when the hydroelectric plant was not in operation, the sample reference statistics for valley streamflows are a coefficient of variation of 0.401, a skewness coefficient of 1.63, and a kurtosis coefficient of 4.68. Table 6 presents results for the considered probability distributions with their corresponding fitting methods. The gray cells represent the best fit of the dataset.

Based on the statistical criteria of Chi-square, coefficients of variation, skewness coefficients, and kurtosis coefficients demonstrating the best fit with the data, the probability distribution of Weibull was preselected using the maximum likelihood fitting, maximum likelihood gamma, and maximum likelihood adjusted log-normal methods for comparison between their AIC values during 1972–1999, a time when the hydroelectric plant was not yet in operation.

Based on the above, and with the aim of objectively choosing the best fit for the probability distribution, a comparison of Akaike criteria was performed. For the period of 1972–1999, the maximum likelihood Weibull, maximum likelihood gamma, and maximum likelihood adjusted log-normal yield AIC values of 260.12, 253.82, and 251.25, respectively. Therefore, for the projections of different return periods of river drought flows during 1972–1999, the log-normal probability distribution was chosen using the maximum likelihood adjusted method.

Similarly, for the period of 2000–2021, when the hydroelectric plant was in operation, the sample reference statistics for valley streamflows are a coefficient of variation of 0.358, a skewness coefficient of −0.264, and a kurtosis coefficient of 1.19. To objectively choose the best fit for the probability distribution, a comparison of Akaike criteria was performed. For the period from 2000 to 2021, Weibull maximum likelihood, log Pearson type III method of moments, and gamma by the method of moments yield AIC values of 222.36, 221.14, and 224.40, respectively. Therefore, for the projections of different return periods of river drought flows for the period from 2000 to 2021, the log Pearson type III distribution by the

method of moments (BOB) is chosen. Considering the selected probability distributions with their methods, the projected valley streamflows or minimum drought flows for different return periods are provided for the periods from 1972 to 1999 and from 2000 to 2021. The higher the return period, the lower the values of streamflow achieved for both analyzed periods, as shown in Table 7 and Figure 11.

Table 6. Statistics of probability distributions used in the analysis of observed valley flows from 1972 to 1999.

Probability Dist.	Fitting Method	Statistics			
		X^2	C_v	C_s	C_k
Weibull	MV	9.56	0.411	0.308	2.81
	MM	9.56	0.041	0.279	2.79
GEV	MVA	1.26	0.43	3.6	51.3
	MM	4.37	0.401	1.63	8.51
	MMP	2.81	0.454	4.54	14.3
Gumbel	MVA	1.26	0.346	1.14	2.4
	MM	3.33	0.401	1.14	2.4
	MMP	2.3	0.385	1.14	2.4
Normal	MVA	9.04	0.401	0	3
Log-normal	MVA	1.26	0.362	1.13	5.36
Three-parameter log-normal	MVA	3.33	0.4	2.17	12.4
	MM	4.37	0.401	1.63	8.1
Gamma	MV	1.78	0.353	0.707	3.75
	MM	5.41	0.401	0.802	3.96
Inverse Gamma	MV	2.3	0.37	1.72	9.38
Generalized Gamma	MV	209.3	0.433	3.94	91.3
	MM	219.5	0.401	1.63	8.53
Pearson type III	MV	3.85	0.38	1.46	6.19
	MM	5.41	0.401	1.63	7.01
Log Pearson type III	SAM	2.81	0.404	2.4	17.4
	BOB	3.85	0.393	1.54	7.76
	WRC	3.33	0.42	2.7	21.1

Table 7. Valley flows for return periods of 1970–1999 and 2000–2021.

Tr (Years)	$Q_{V,Tr}$ (m^3/s)			
	Before the Operation of the Hydropower Plant	After the Operation of the Hydropower Plant		
	1970–1999	2000–2021	2000–2010	2011–2021
500	25.00	12.30	35.40	117.00
100	30.30	21.90	39.50	120.00
50	33.30	28.20	41.80	122.00
20	38.50	39.80	45.50	124.00
10	43.70	52.00	49.20	126.00
5	51.00	68.90	54.30	129.00

Two operational regimes were observed in the Urrá 1 hydroelectric plant, and then the authors statistically assessed the data in two periods: 2000–2010 and 2011–2021. The probability distribution of inverse gamma by the maximum likelihood method was chosen for the projections of drought flows for different return periods of the river for the period from 2000 to 2010, and for the period from 2011 to 2021, the probability distribution of gamma by the method of moments was chosen. The gray cells in Table 7 show the selected values of minimum flow associated with different return periods. The analysis from

the entire period of 2000–2021 should be neglected since the hydropower plant had two operational regimes that were considered for hydrological analysis.

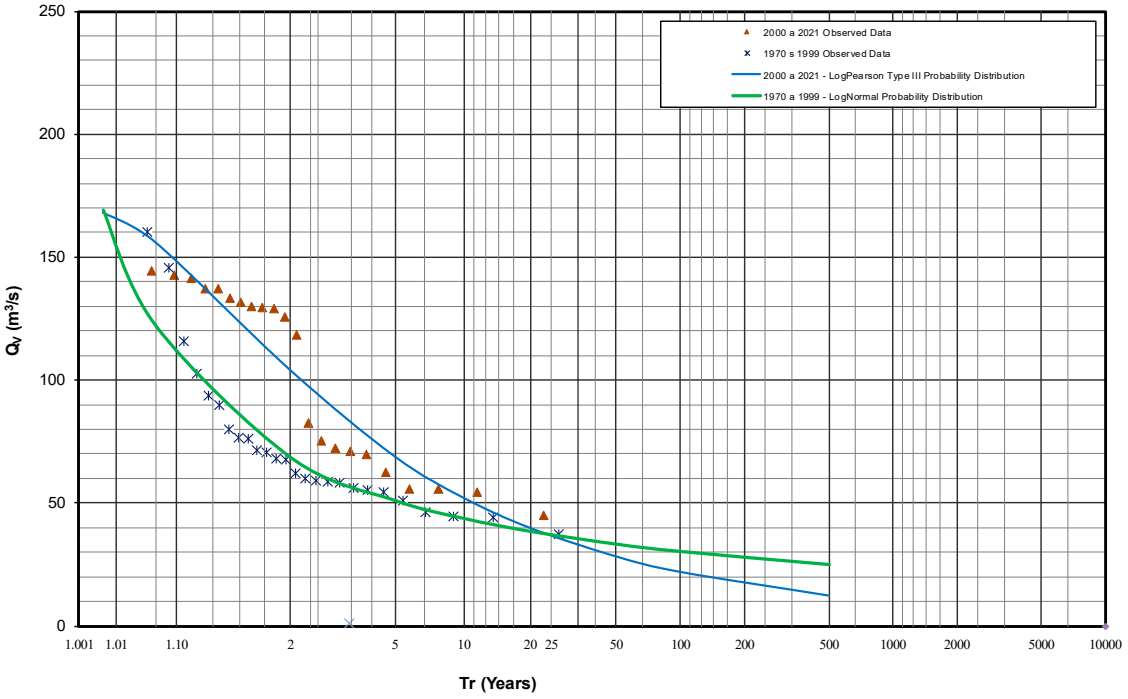

(**a**)

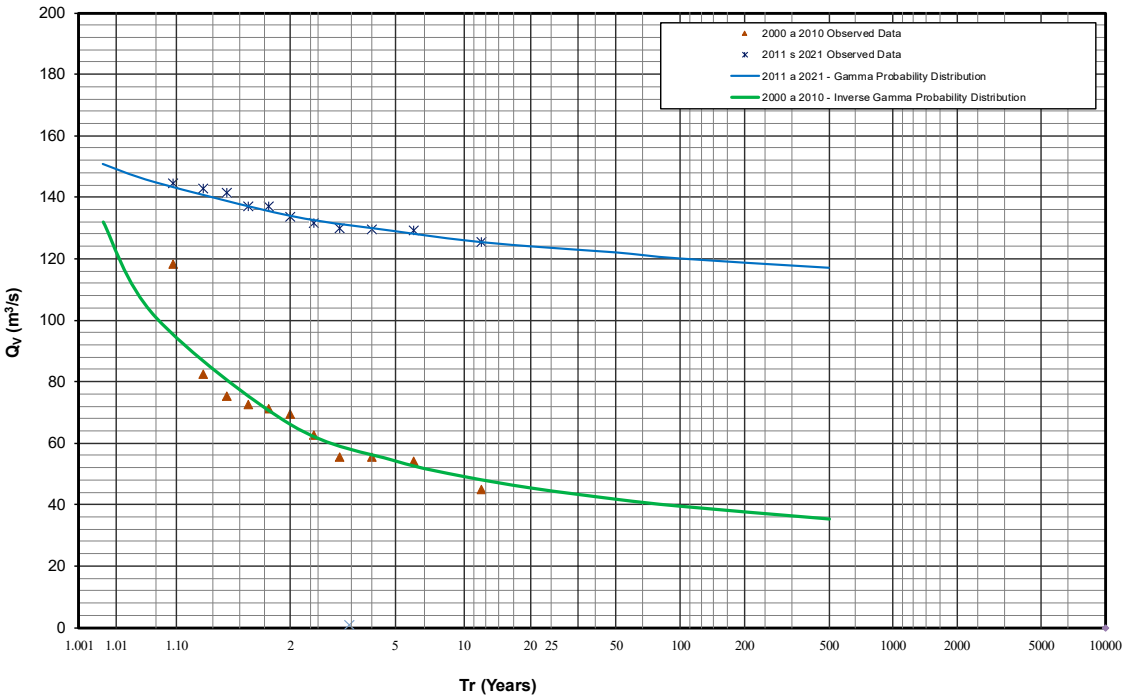

(**b**)

Figure 11. Recorded valley streamflows versus projections for different return periods: (**a**) from 1970 to 1999 and 2000 to 2021; and (**b**) from 2000 to 2010 and 2011 to 2021.

4.2.2. Drought Durations D_S of the Sinú River

For the period from 1972 to 1999, when the hydroelectric plant was not in operation, the gamma distribution by the maximum likelihood method was chosen for projections at different return periods of drought durations in the river for the period from 1972 to 1999, following the same procedure described in Section 4.2.1. Here, for the analysis of drought durations in the period from 1970 to 1999, the years 1970 and 1971 were not considered due to insufficient data to represent the hydrological behavior of the river during that time span. The analysis for the entire period from 2000–2021 was not considered for the two operational regimes of the hydropower plant. In a similar fashion to what was carried out for streamflows, the authors performed the same statistical analysis for drought durations, obtaining the following results for the periods from 2000 to 2010 and 2011 to 2021, where the gamma distribution by the maximum likelihood method was selected for both periods. Table 8 and Figure 12 present the results of drought duration for different return periods.

Table 8. Drought durations, D_{STr}, for different return periods: 1970–1999, 2000–2010, and 2011–2021.

Tr	$D_{S,Tr}$ (Day)		
	Before the Operation of the Hydropower Plant	After the Operation of the Hydropower Plant	
	1970–1999	2000–2010	2011–2021
500	155.00	67.70	86.50
100	124.00	55.50	70.50
50	111.00	50.10	63.30
20	92.00	43.50	53.40
10	77.30	36.40	45.40
5	61.60	29.90	36.90

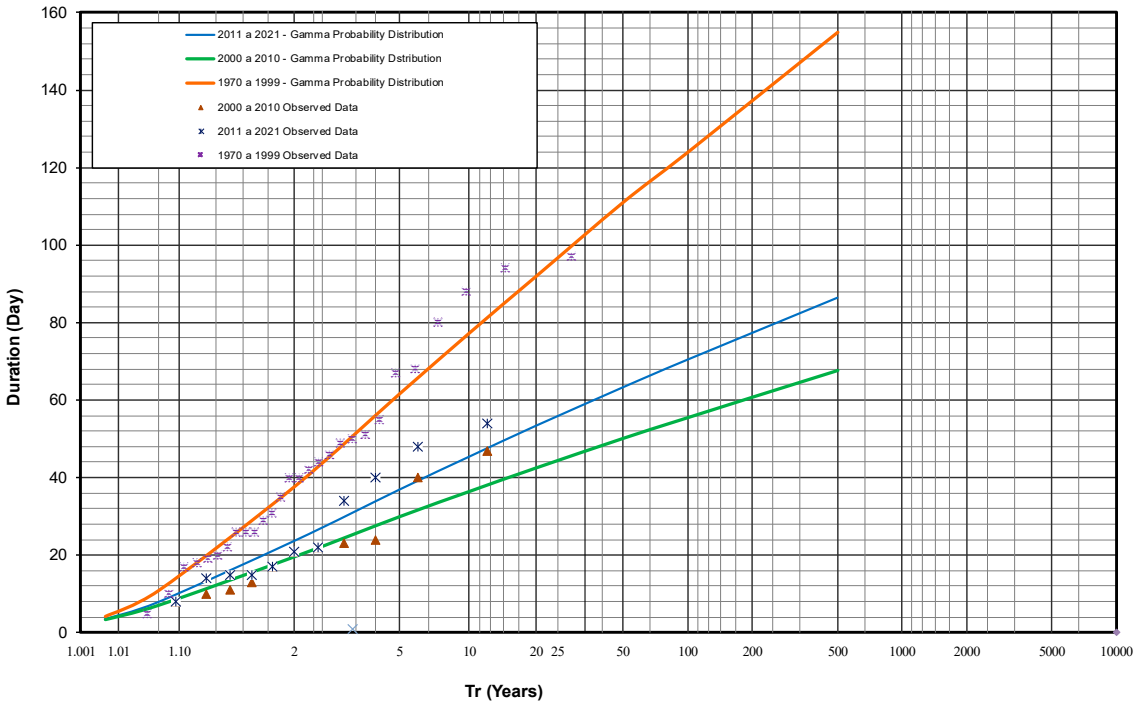

Figure 12. Recorded drought duration versus duration for the different return periods: 1970–1999, 2000–2010, and 2011–2021.

5. Discussion

Electric power generation plants relying on water accumulation can either provide solutions or present challenges, contingent on the philosophy guiding the operational

policies of the plant. The operational policies of energy generation must be modified and should take into account the sustainability of river ecosystems, as well as the preservation of human life directly threatened by the lack of water to meet their basic needs [30]. In addition, the operation of the hydroelectric plant should be viewed beyond the energy focus, considering the social responsibility it holds by impacting the sustainability of the communities present in the territory.

In the pursuit of the initial specific objective, comprehensive flow data from the Montería Automatic station were collected. An examination of the base flows revealed a discernible impact of the Urrá 1 hydroelectric plant, leading to a notable augmentation in the average river flows. This is attributed to a shift in the operational policies of the plant, wherein the minimum river flows since 2011 have exhibited a substantially higher magnitude, nearly double that in the initial decade of the hydroelectric plant's operation. While this has positively influenced the minimum river streamflows, Q_V, it has kept drought durations, D_S, slightly higher in the latter period. These observed values undeniably influenced the projections of minimum flows for several return periods, Q_{VTr}, and drought durations, D_{STr}, across different return periods.

The minimum flows for diverse return periods are listed in Table 7. For the period 2011–2021, the minimum flow values surpass those of the other periods, ranging from 117.00 m^3/s for 500 years to 129.00 m^3/s for 5 years. The 2000–2021 period exhibits flows ranging from 12.30 m^3/s to 68.90 m^3/s, in which the hydroelectric plant is operational with distinct operating regimes.

The minimum flows for various return periods are found in Table 7. For the period 2011–2021, the minimum flow values surpass those of other periods, being 122.00 m^3/s for a 50-year return period and 129.00 m^3/s for 5 years. The period from 2000 to 2021 has minimum flows of 28.20 m^3/s for a 50-year return period and 68.90 m^3/s for a 5-year occurrence probability, in which the hydroelectric plant is operational with different operating regimes. When comparing the period from 1972 to 1999 with that of 2011 to 2021, we see that the current operational conditions favor an increase in the minimum flow, placing it 88.70 m^3/s above what would be obtained for a 50-year return period under natural hydrological conditions.

Regarding drought durations, D_{STr}, Table 8 reveals that in 2000–2021, i.e., when the Urrá 1 hydroelectric plant was in operation, the drought durations were shorter than those in 1972–1999. The latter period represents the natural hydrological and hydraulic conditions of the Sinú River, underscoring that the hydroelectric plant's operation acts as a mitigating factor in reducing the duration of drought days in the river.

Furthermore, for a return period of 50 years, a reduction in drought durations of 47.70 days is expected, corresponding to a 42.97% reduction. For a return period of 5 years, there is a reduction of 24.70 days, equivalent to a 40.09% reduction. This comparison is made between the natural hydrological and hydraulic conditions in 1972–1999 and the current operational conditions of the hydroelectric plant (2011–2021). The reductions in drought durations are significant and occur due to the operation of the hydroelectric plant. It is worth noting that, in the operational regime from 2000 to 2010, drought durations are shorter than those projected for the period from 2011 to 2021, clearly indicating that the operation of the hydroelectric plant can considerably mitigate the durations of droughts and the impacts they cause in the region.

The results obtained show an increase in the severity of drought durations with the possibility of occurrence for longer return periods. This makes it imperative for riverside communities and governmental establishments to establish risk mitigation policies where, from now on, strategies are designed to preserve human and wildlife life from the impact of droughts. Extended periods of hydrological drought result in a continuous decrease in the level of moisture present in the soil [31].

The operation of the hydroelectric plant, given its confirmed direct impact on maximum, mean, and minimum river flows, should not be solely regarded from the perspective of electricity generation. Alternatively, a comprehensive viewpoint considering the ecosys-

tem sustainability of the territories is advocated. As demonstrated in this study, the operation of the hydroelectric plant has the potential to positively influence both sectors efficiently. The knowledge shared herein contributes to a better understanding of the current interrelation among the Sinú River basin, the Urrá 1 hydroelectric plant, and the communities residing within the territories.

The results of flow projections for the period from 1972 to 1999 indicate that for a return period of 500 years, there is a drastic decrease in minimum streamflows, Q_{VTr}, reaching around 25.00 m^3/s. This presents the possibility of an extreme drought that could jeopardize the sustainability of ecosystems and riverside communities dependent on the river. For the period between 2000 and 2021, considering it in its entirety, the drought flow for a return period of 500 years is 12.30 m^3/s, indicating an even more extreme drought. During this period, the Urrá 1 hydroelectric plant was in operation. However, when segmenting the period from 2000 to 2021 based on the plant's operational policies, the projected flows for 500 years are 35.40 m^3/s for the period from 2000 to 2010 and 117.00 m^3/s for the period from 2011 to 2021. This leads to the conclusion that the operational policies of the hydroelectric plant significantly impact the minimum drought flows in the river, potentially providing the necessary flows to mitigate the risk of extreme droughts in the middle and lower river basins. Still, we must note that similar trends were observed in the other return periods assessed in this research study.

Concerning drought durations, for a return period of 500 years, the period from 1972 to 1999 projects an expected drought duration of 155 days, while for the years 2000 to 2021, it is 78 days for the same return period. This underscores that the operation of the hydroelectric plant positively influences drought durations in the river, making them shorter and consequently reducing the negative impact on the territory.

In conclusion, the operation of the hydroelectric plant directly influences minimum river streamflows, Q_{VTr}, and drought durations, D_{STr}, for different return periods, thereby playing a crucial role in water resource management. Moreover, operational policies for energy generation should not overlook downstream impacts, as they directly affect the risk of extreme droughts in the middle and lower river basins.

Author Contributions: Conceptualization, A.F.V.-B., A.A.-P. and O.E.C.H.; methodology, H.M.R. and V.S.F.-M.; formal analysis, A.F.V.-B., A.A.-P. and O.E.C.H.; investigation, A.F.V.-B., O.E.C.H., H.M.R. and V.S.F.-M.; writing—original draft preparation, A.F.V.-B. and O.E.C.H.; supervision, A.A.-P., H.M.R. and V.S.F.-M. All authors have read and agreed to the published version of the manuscript.

Funding: This research project did not receive external or internal funding.

Institutional Review Board Statement: Not applicable.

Informed Consent Statement: Not applicable.

Data Availability Statement: The raw data supporting the conclusions of this article will be made available by the authors on request.

Conflicts of Interest: The authors declare no conflicts of interest.

Appendix A

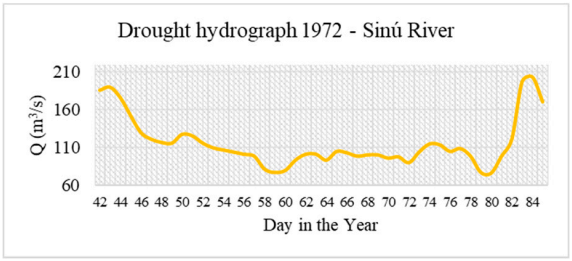

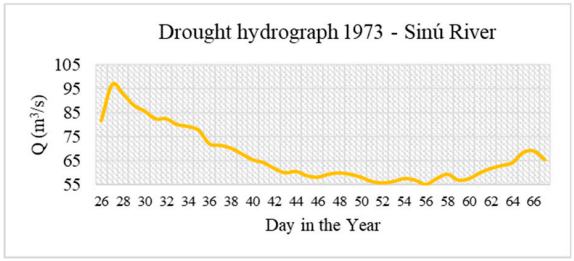

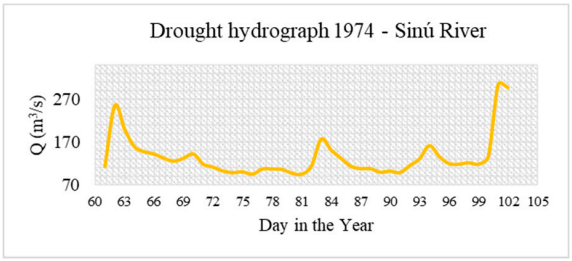

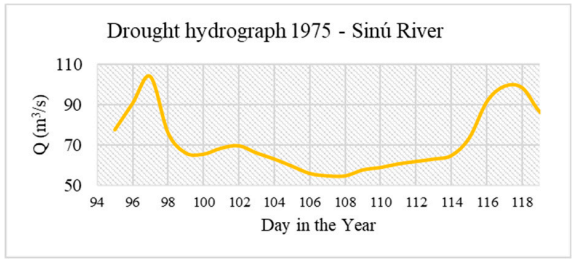

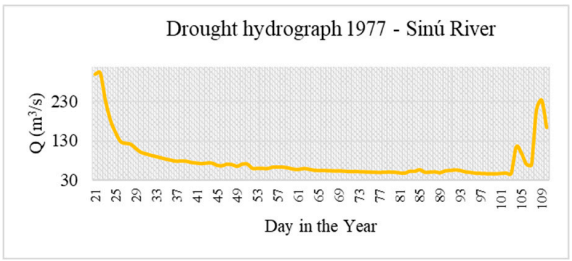

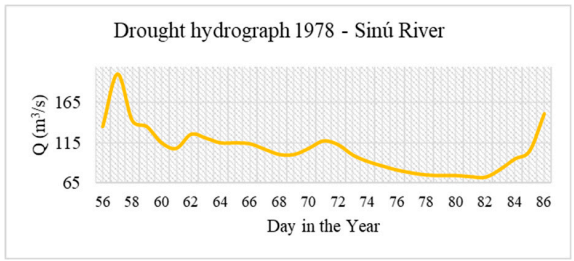

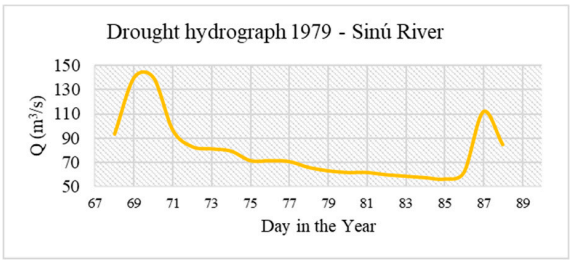

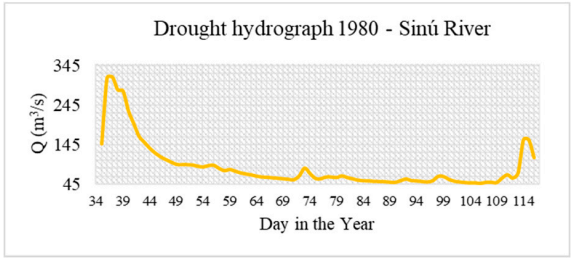

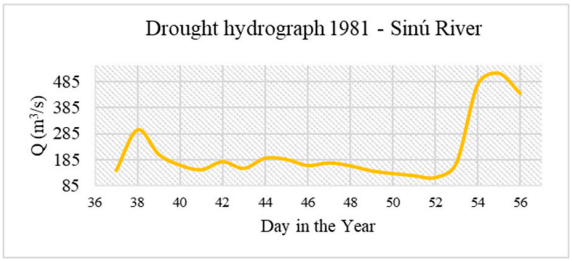

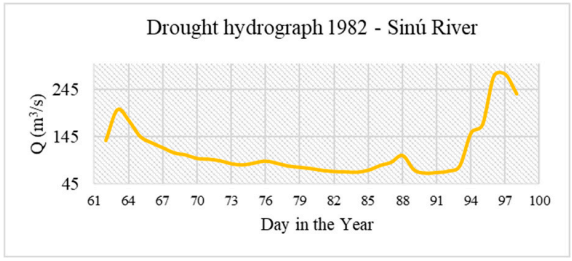

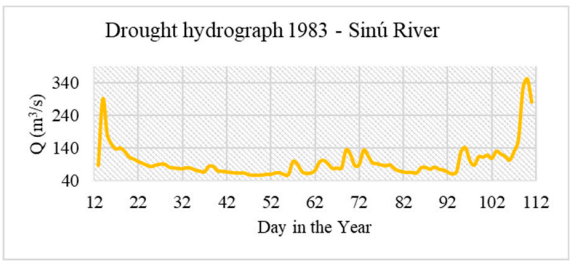

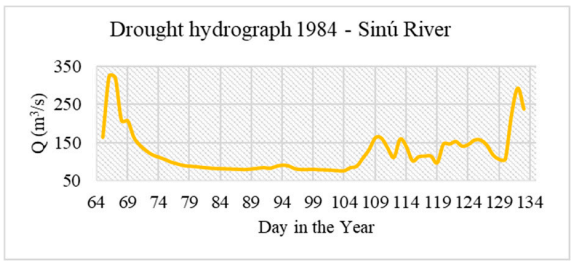

Figure A1. *Cont.*

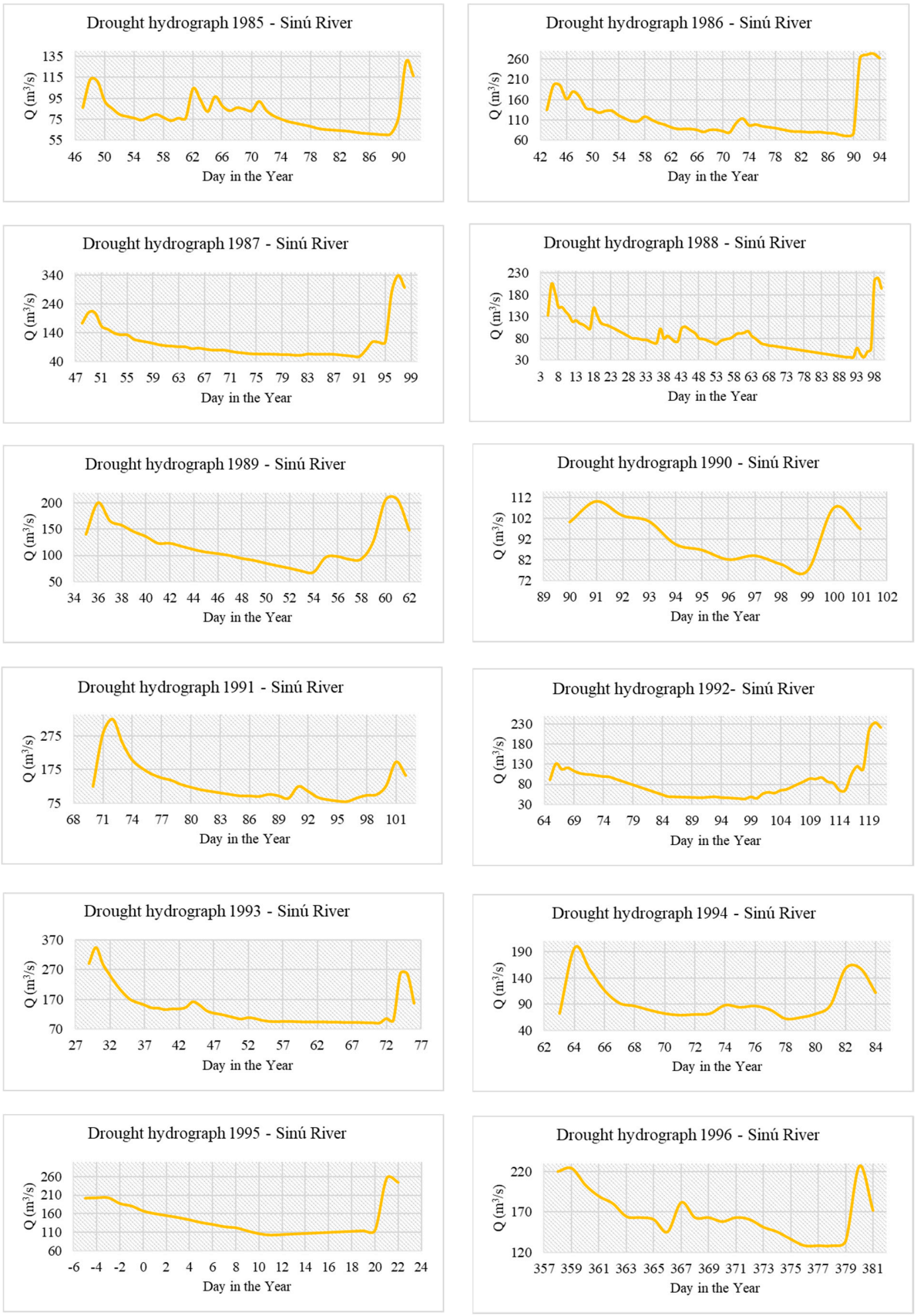

Figure A1. *Cont.*

Figure A1. *Cont.*

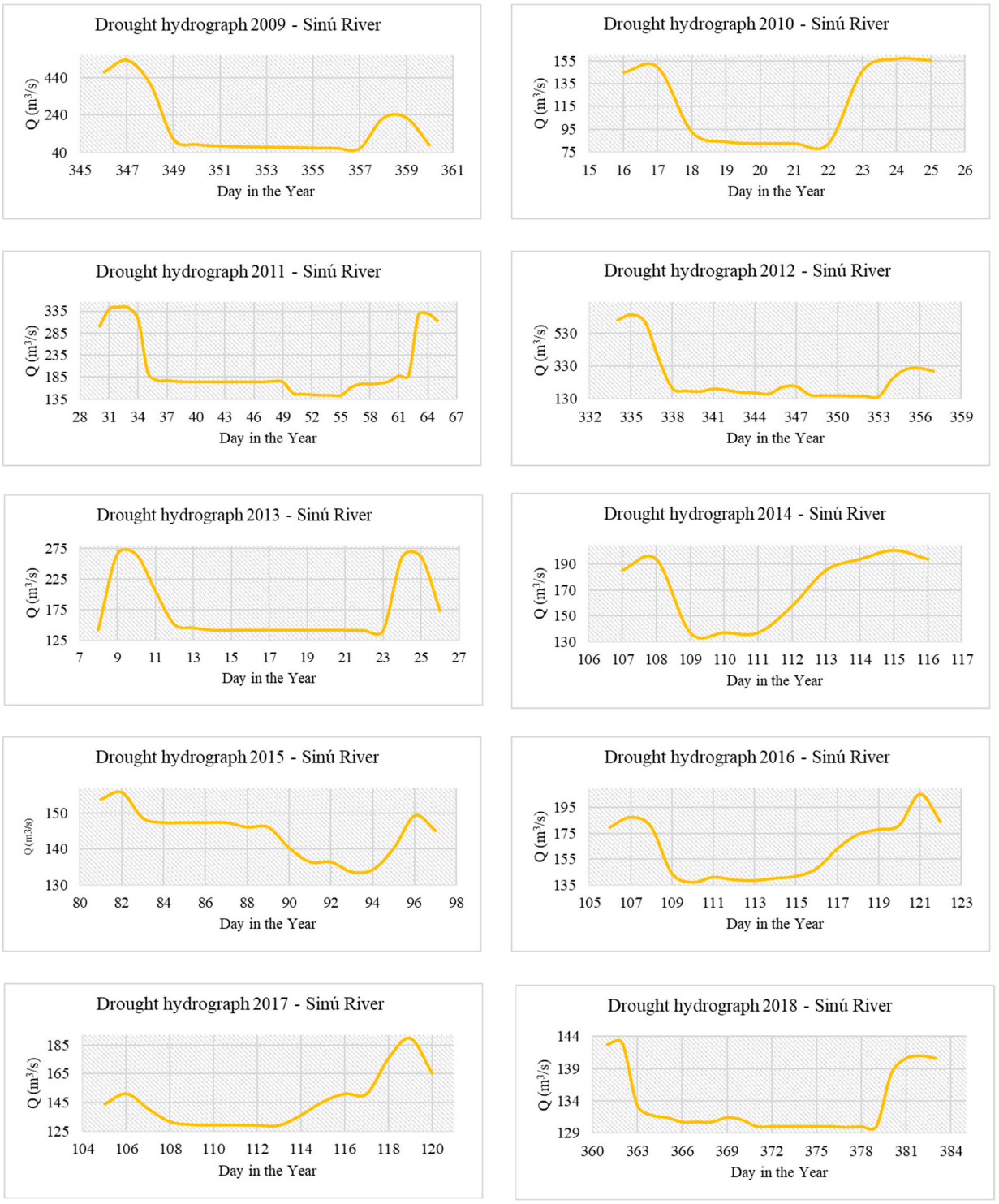

Figure A1. *Cont.*

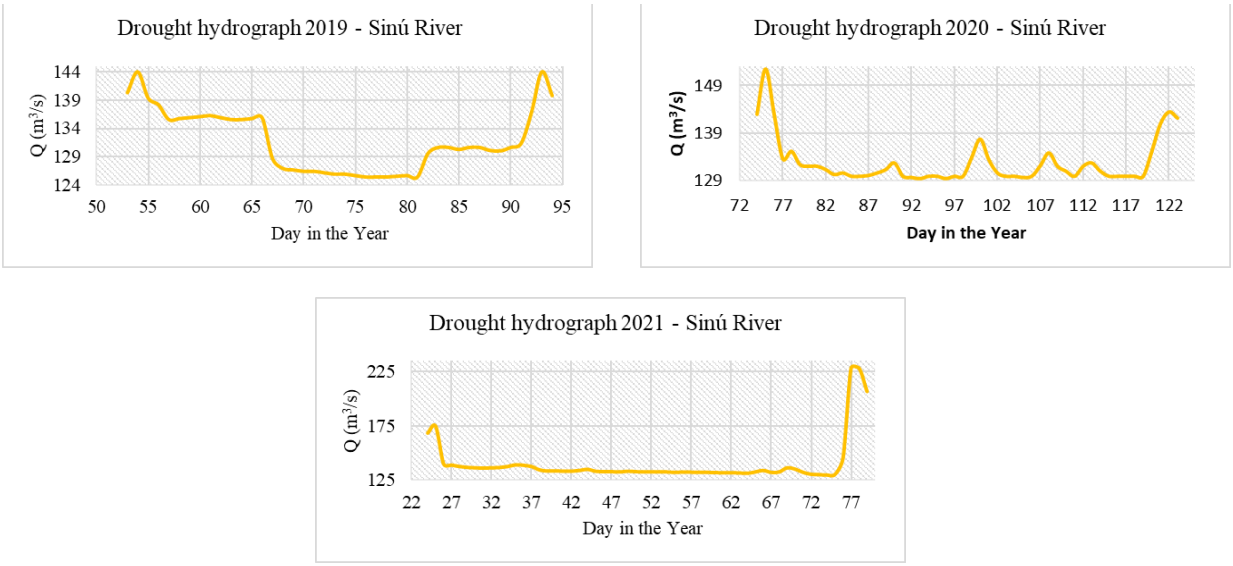

Figure A1. Complete record of annual drought hydrographs registered at the Montería Automatic station from 1972 to 2021.

References

1. Brubaker, K.L.; Entekhabi, D.; Eagleson, P.S. Estimation of continental precipitation recycling. *J. Clim.* **1993**, *6*, 1077–1089. [CrossRef]
2. Entekhabi, D.; Rodriguez-Iturbe, I.; Bras, R.L. Variability in large-scale water balance with land surface-atmosphere interaction. *J. Clim.* **1992**, *5*, 798–813. [CrossRef]
3. Namias, J. Some causes of United States drought. *J. Appl. Meteorol. Climatol.* **1983**, *22*, 30–39. [CrossRef]
4. Yang, G.; Block, P. Enhancing season-ahead streamflow forecasts with GCMs, climate indices, and their interactions. *J. Water Resour. Plan. Manag.* **2023**, *149*, 04023055. [CrossRef]
5. Wong, G.; Van Lanen, H.A.J.; Torfs, P.J.J.F. Probabilistic analysis of hydrological drought characteristics using meteorological drought. *Hydrol. Sci. J.* **2013**, *58*, 253–270. [CrossRef]
6. Sun, H.; Sun, X.; Chen, J.; Deng, X.; Yang, Y.; Qin, H.; Chen, F.; Zhang, W. Different types of meteorological drought and their impact on agriculture in Central China. *J. Hydrol.* **2023**, *627*, 130423. [CrossRef]
7. Rind, D.; Goldberg, R.; Hansen, J.; Rosenzweig, C.; Ruedy, R. Potential evapotranspiration and the likelihood of future drought. *J. Geophys. Res. Atmos.* **1990**, *95*, 9983–10004. [CrossRef]
8. Palmer, W.C. *Meteorological Drought*; US Department of Commerce, Weather Bureau: Washington, DC, USA, 1965; Volume 30.
9. Karl, T. *Atlas of Monthly Palmer Moisture Anomaly Indices (1895–1930) for the Contiguous United States (Volume 3, No. 8–9)*; National Climatic Data Center: Asheville, NC, USA, 1985.
10. Karl, T. *Atlas of Monthly Palmer Hydrological Drought Indices (1931–1983) for the Contiguous United States (Volume 3)*; National Climatic Data Center: Asheville, NC, USA, 1985.
11. Rajsekhar, D.; Singh, V.P.; Mishra, A.K. Hydrologic drought atlas for Texas. *J. Hydrol. Eng.* **2015**, *20*, 05014023. [CrossRef]
12. Chow, V.T.; Maidment, D.R.; Mays, L.W. *Applied Hydrology*; McGraw-Hill: New York, NY, USA, 1988.
13. Villalba-Barrios, A.F.; Coronado-Hernández, O.E.; Fuertes-Miquel, V.S.; Coronado-Hernández, J.R.; Ramos, H.M. Statistical Approach for Computing Base Flow Rates in Gaged Rivers and Hydropower Effect Analysis. *Hydrology* **2023**, *10*, 137. [CrossRef]
14. Gupta, S.C.; Kapoor, V.K. *Fundamentals of Mathematical Statistics*; Sultan Chand & Sons: Delhi, India, 2020.
15. Nguyen, H.T.; Rogers, G.S. *Fundamentals of Mathematical Statistics: Probability for Statistics*; Springer Science & Business Media: Berlin/Heidelberg, Germany, 2012.
16. Archer, D.; Foster, M.; Faulkner, D.; Mawdsley, J. The synthesis of design flood hydrographs. In *Proceedings of the ICE/CIWEM Conf. Flooding–Risks and Reactions*; Terrace Dalton: London, UK, 2000.
17. Weibull, W. A statistical distribution function of wide applicability. *J. Appl. Mech.* **1951**, *18*, 293–297. [CrossRef]
18. Coles, S.; Bawa, J.; Trenner, L.; Dorazio, P. *An Introduction to Statistical Modeling of Extreme Values*; Springer: London, UK, 2001; Volume 208, p. 208.
19. Gumbel, E.J. *Statistics of Extremes*; Courier Corporation: North Chelmsford, MA, USA, 2004.
20. Grego, J.M.; Yates, P.A. Point and standard error estimation for quantiles of mixed flood distributions. *J. Hydrol.* **2010**, *391*, 289–301. [CrossRef]
21. Coronado-Hernández, Ó.E.; Merlano-Sabalza, E.; Díaz-Vergara, Z.; Coronado-Hernández, J.R. Selection of hydrological probability distributions for extreme rainfall events in the regions of Colombia. *Water* **2020**, *12*, 1397. [CrossRef]

22. El Adlouni, S.; Bobée, B. Hydrological Frequency Analysis Using HYFRAN-PLUS Software. User's Guide Available with the Software DEMO. 2015. Available online: http://www.wrpllc.com/books/HyfranPlus/indexhyfranplus3.html (accessed on 8 August 2023).
23. Seckin, N.; Yurtal, R.; Haktanir, T.; Dogan, A. Comparison of probability weighted moments and maximum likelihood methods used in flood frequency analysis for Ceyhan River Basin. *Arab. J. Sci. Eng.* **2010**, *35*, 49.
24. Ji, X.; Jing, D.; Shen, H.W.; Salas, J.D. Plotting positions for Pearson type-III distribution. *J. Hydrol.* **1984**, *74*, 1–29.
25. Greis, N.P. Flood frequency analysis: A review of 1979–1982. *Rev. Geophys.* **1983**, *21*, 699–706. [CrossRef]
26. Chatfield, C. *Statistics for Technology: A Course in Applied Statistics*; Routledge: London, UK, 2018.
27. Tong, Y.L. *Engineering Statistics*; Mathematics for Mechanical Engineers; Taylor and Francis Group: New York, NY, USA, 2022; pp. 11-1–11-12.
28. Wagenmakers, E.J.; Farrell, S. AIC model selection using Akaike weights. *Psychon. Bull. Rev.* **2004**, *11*, 192–196. [CrossRef] [PubMed]
29. Obeysekera, J.; Salas, J. Hydrologic designs for extreme events under nonstationarity. In *Engineering Methods for Precipitation under a Changing Climate*; Florida International University: Miami, FL, USA, 2020; pp. 63–82.
30. Paredes-Trejo, F.; Olivares, B.O.; Movil-Fuentes, Y.; Arevalo-Groening, J.; Gil, A. Assessing the Spatiotemporal Patterns and Impacts of Droughts in the Orinoco River Basin Using Earth Observations Data and Surface Observations. *Hydrology* **2023**, *10*, 195. [CrossRef]
31. Geng, G.; Zhang, B.; Gu, Q.; He, Z.; Zheng, R. Drought propagation characteristics across China: Time, probability, and threshold. *J. Hydrol.* **2024**, *631*, 130805. [CrossRef]